

**NOTE • OPEN ACCESS**

## Histological assessment of a chronically implanted cylindrically-shaped, polymer-based neural probe in the monkey

To cite this article: M Gerbella *et al* 2021 *J. Neural Eng.* **18** 024001

View the [article online](#) for updates and enhancements.



## NOTE

## Histological assessment of a chronically implanted cylindrically-shaped, polymer-based neural probe in the monkey

## OPEN ACCESS

## RECEIVED

9 December 2020

## ACCEPTED FOR PUBLICATION

18 January 2021

## PUBLISHED

26 February 2021

Original content from this work may be used under the terms of the [Creative Commons Attribution 4.0 licence](#).

Any further distribution of this work must maintain attribution to the author(s) and the title of the work, journal citation and DOI.



M Gerbella<sup>1</sup> , E Borra<sup>1</sup> , F Pothof<sup>2</sup>, M Lanzilotto<sup>3</sup> , A Livi<sup>5</sup> , L Fogassi<sup>1</sup> , O Paul<sup>2,4</sup> , G A Orban<sup>1</sup> , P Ruther<sup>2,4</sup> and L Bonini<sup>1</sup>

<sup>1</sup> Dipartimento di Medicina e Chirurgia, Università degli Studi di Parma, Parma, IT, Italy

<sup>2</sup> Department of Microsystems Engineering (IMTEK), University of Freiburg, Freiburg, DE, Germany

<sup>3</sup> Department of Psychology, University of Turin, Turin, IT, Italy

<sup>4</sup> BrainLinks-BrainTools, University of Freiburg, Freiburg, DE, Germany

<sup>5</sup> Department of Neuroscience, Washington University, St. Louis, MO 63110, United States of America

E-mail: [marzio.gerbella@unipr.it](mailto:marzio.gerbella@unipr.it)

**Keywords:** focal epilepsy, stereoelectroencephalography, SEEG, histocompatibility, chronic probes

**Abstract**

**Objective.** Previous studies demonstrated the possibility to fabricate stereo-electroencephalography probes with high channel count and great design freedom, which incorporate macro-electrodes as well as micro-electrodes offering potential benefits for the pre-surgical evaluation of drug resistant epileptic patients. These new polyimide probes allowed to record local field potentials, multi- and single-unit activity (SUA) in the macaque monkey as early as 1 h after implantation, and yielded stable SUA for up to 26 d after implantation. The findings opened new perspectives for investigating mechanisms underlying focal epilepsy and its treatment, but before moving to possible human application, safety data are needed. In the present study we evaluate the tissue response of this new neural interface by assessing post-mortem the reaction of brain tissue along and around the probe implantation site. **Approach.** Three probes were implanted, independently, in the brain of one monkey (*Macaca mulatta*) at different times. We used specific immunostaining methods for visualizing neuronal cells and astrocytes, for measuring the extent of damage caused by the probe and for relating it with the implantation time. **Main results.** The size of the region where neurons cannot be detected did not exceed the size of the probe, indicating that a complete loss of neuronal cells is only present where the probe was physically positioned in the brain. Furthermore, around the probe shank, we observed a slightly reduced number of neurons within a radius of 50  $\mu\text{m}$  and a modest increase in the number of astrocytes within 100  $\mu\text{m}$ . **Significance.** In the light of previous electrophysiological findings, the present data suggest the potential usefulness and safety of this probe for human applications.

**1. Introduction**

Recording electrical activity from the brain is of critical importance in the case of several human neurological disorders, for diagnosing and treating them [1, 2] as well as to collect fundamental data about brain mechanisms underlying motor, perceptual and cognitive functions [3–5]. Recent developments in probe technologies for experimental applications in animal models enabled the improvement of both the quality and stability of recorded signals [6–9] as well as to achieve intracortical electrical [10] and optical [11, 12] stimulation capabilities. However, the technology of deep brain probes is much less

advanced for human applications and is essentially limited to a few neural devices containing only a small number of macroelectrodes [1, 2] and, sometimes, microelectrodes [13–16]. These devices offer a spatial resolution which is largely insufficient to simultaneously monitor the spiking activity of many individual neurons.

Recently, to maximally exploit the potential of human intracortical recordings, novel, cylindrically shaped neural probes consisting of a high number of microelectrodes capable to record local field potentials (LFP), multi-unit (MUA) and single-unit (SUA) activity, have been developed and physiologically validated in the monkey [6]. The findings demonstrated

that these probes can record LFP and MUA as early as 1 h after implantation and provide, in addition, stable SUA signals for up to 26 d after implantation.

In view of their possible application for monitoring neuronal activity in humans, combining clinical needs of sampling stereo-electroencephalography (SEEG) signal with experimental desires of recording SUA and MUA simultaneously, these high-channel-count recording devices have been fabricated in a biocompatible material, i.e. polyimide (PI) [6, 17–19]. However, a previous electrophysiological validation study in monkey [6] did not provide evidence about the actual effect of these neural devices on the tissue, which is to date limited to evidence of chronic applications of shorter probes of the same outer diameter in the rat [20].

To fill this gap and to directly assess the astroglia reaction and neuronal degeneration caused by cylindrical probes similar in length to those used in human patients [21–23], we analyzed post-mortem brain tissue of the macaque monkey previously involved in the electrophysiological validation of these probes [6]. The monkey is an optimal model because its brain size allows the implantation protocol to faithfully reproduce that of humans. Preliminary neurophysiological recordings were made for periods equal to or even longer than those required for preclinical evaluation of epileptic patients (from 1 to 2 weeks). Three probes have been implanted at different times, two of them about 1 year and the third one about 1 month before euthanizing the animal. The histological and immunohistochemical analysis of the cortical tissue around the probes showed that: (a) the size of the mechanical lesion caused by the implantation did not exceed the diameter of the probes (800  $\mu\text{m}$ ) and (b) the loss of neurons and glial reaction were limited to a radius of 50  $\mu\text{m}$  and 100  $\mu\text{m}$  around the probe shank, respectively.

## 2. Material and methods

### 2.1. Probe technology

The PI-based SEEG probes used in this study (figure 1) have an outer diameter of 800  $\mu\text{m}$  and length of 22 mm and comprise 32 or 64 electrode sites. They have been described in detail elsewhere [6]. In short, PI-based probe substrates comprising electrodes implemented as small disks (microelectrodes) and cylinders (macroelectrodes), their respective wiring and contact pads made from a thin layer of platinum (Pt) sandwiched between two 5  $\mu\text{m}$  thin layers of PI are realized using microfabrication processes such as spin-coating, sputter deposition and dry etching. The electrodes are implemented either as microelectrodes with a diameter of 35  $\mu\text{m}$ , or macroelectrodes with a surface area of 4.2 mm<sup>2</sup>. The PI substrates are transferred into hollow cylinders with an outer diameter of 800  $\mu\text{m}$  using a three-dimensional shaping process which applies a custom-designed

mold. The hollow probe cylinders are subsequently filled with a biocompatible polymer to increase their mechanical stability.

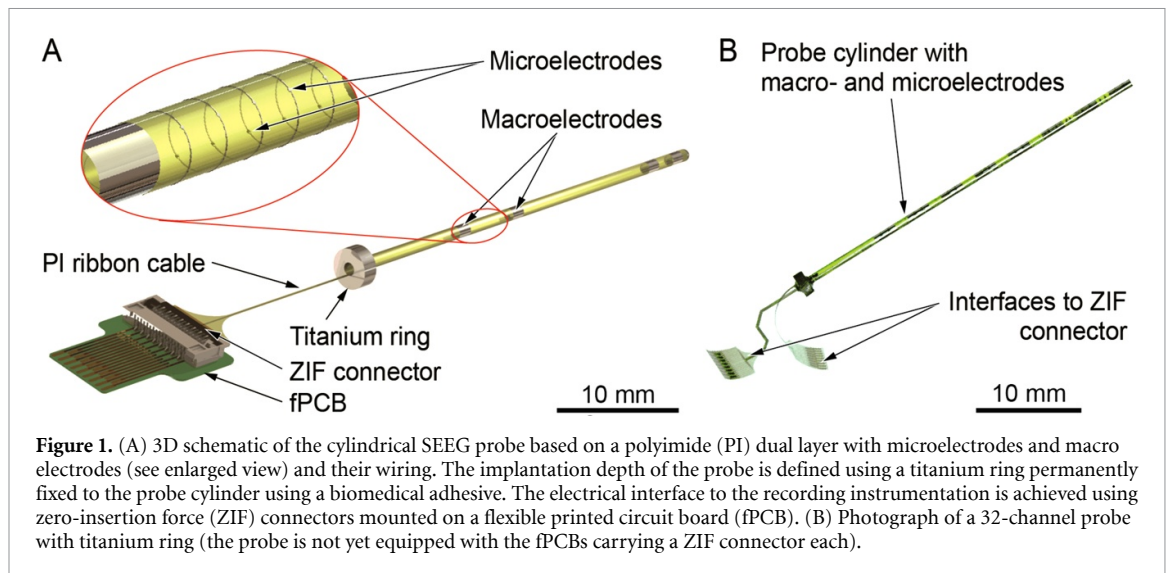
### 2.2. Animal handling

Animal handling as well as surgical and experimental procedures complied with the European law on the humane care and use of laboratory animals (Directive 2010/63/EU) and with the Italian laws in force on the protection of animals used for scientific purposes (Dlgs 26/2014). They were approved by the Veterinarian Animal Care and Use Committee of the University of Parma (Prot. 78/12 17/07/2012 and 48/2016-PR, 20/01/2016) and authorized by the Italian Ministry of Health (D.M. 294/2012-C, 11/12/2012 and Prot. 91/OPBA/2015).

### 2.3. Histology

The probes were implanted in the left hemisphere at three different time points with the same surgical procedure used for human patients and described in detail elsewhere for these specific three probes [6]. Probes 1 and 2 have been implanted along the horizontal plane at the level of the superior parietal lobule (Probe 1, figure 2(A)) and of the primary sensory and motor cortex, extending in depth to the cingulate cortex (Probe 2, figure 2(A)). Probe 3 has been implanted through the ventral bank of the intraparietal sulcus extending in depth to the retrosplenial cortex (figure 2(A)). Probe 1 has been explanted after 4 days because of a mechanical damage of the electrical probe connector. Probe 2 remained implanted for 1 month and then was explanted. The explant of these two probes was performed under general anesthesia; the probes were gently removed from the stainless-steel hollow screw through which they were inserted [6]. Probe 3 has been implanted 1 month before euthanizing the animal (1 year after the implantation of Probe 1) and removed post-mortem from the perfused brain. During both, *in-vivo* and *ex-vivo* removal of the probes, inspection using optical microscopy did not evidence any trace of brain tissue on the explanted electrode shank.

After the end of other electrophysiological and neuroanatomical experiments carried out in the other hemisphere [24, 25], the animal was deeply anesthetized and euthanized with an overdose of sodium thiopental, and then perfused through the left cardiac ventricle consecutively with saline (about 2 l in 10 min), 3.5% formaldehyde (5 l in 30 min), and 5% glycerol (3 l in 20 min), all prepared in 0.1 M phosphate buffer with a pH value of 7.4. The head was then blocked coronally on a stereotaxic apparatus and the stainless-steel wires, to which the probes were screwed, were carefully removed from the bone under inspection with a surgical stereo-microscope. Next, the brain was removed from the skull, photographed, and placed in 10% buffered glycerol for 3 days and 20% buffered glycerol for 4 days. Finally, the brain



was cut frozen into coronal sections of  $60\ \mu\text{m}$  in thickness, parallel to the direction of the probe.

The sections were subdivided in five series, in which consecutive sections were spaced  $300\ \mu\text{m}$ . Two series were processed to visualize neuronal nuclei (NeuN) and glial fibrillary acidic protein (GFAP), respectively. Another series was processed with the Nissl method and the remaining two series were used for visualizing neural tracers injected for the purpose of the other aforementioned study [24, 25]. In detail, for each section processed for GFAP and NeuN, endogenous peroxidase activity was eliminated by incubation in a solution of 0.3% hydrogen peroxide and 80% methanol for 15 min at room temperature. The sections were then incubated for 72 h at  $4\ ^\circ\text{C}$  in a primary antibody solution of monoclonal mouse antibody against GFAP (1:2000, EMD Millipore, Merck KGaA, Darmstadt, Germany) or of rabbit NeuN (1:5000, Cell Signaling Technology, Danvers, MA) in phosphate buffer solution containing 0.3% triton and 5% serum. Subsequently, the sections were incubated for 1 h in biotinylated secondary antibody (1:200, Vector Laboratories, Burlingame, CA) in the same phosphate buffer solution (0.5% serum). Finally, GFAP or NeuN positive cells were visualized using the Vectastain ABC kit and diaminobenzidine as a chromogen.

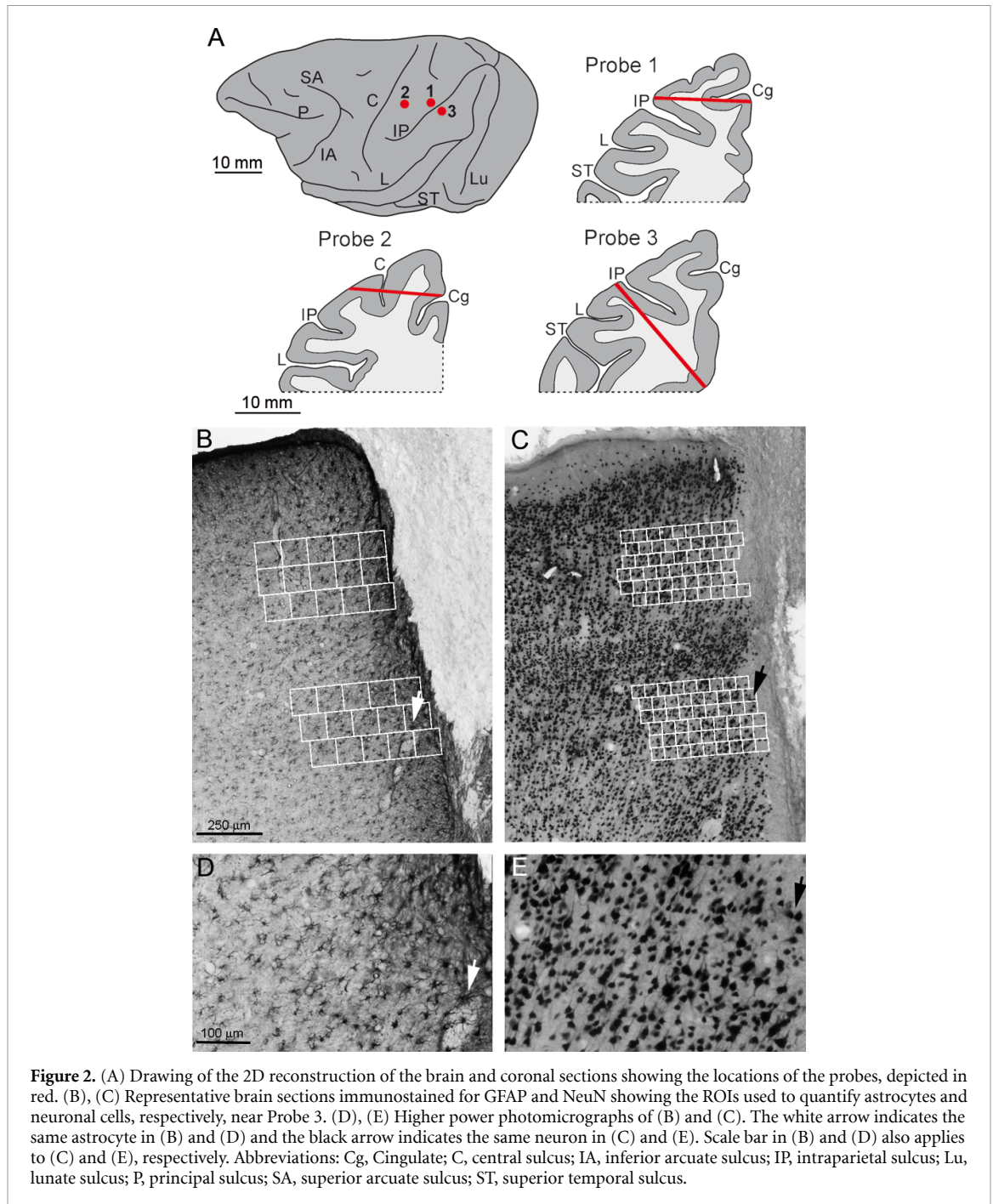
#### 2.4. Analysis of immunostained and Nissl stained sections

The size of the lesions caused by the insertion of the probes, as well as the amount of astroglial reaction and the loss of neurons, were investigated on Nissl-stained and immunostained sections.

For each probe, Nissl-, GFAP- and NeuN-stained sections around the probe location, that is a territory covering locations from 2 mm anterior to 2 mm posterior relative to the insertion track of the probe, were selected and photographed for the analysis. We opted for these methods because we had

two series of brain slices available, as the others were destined to a neuroanatomical tracing study [24]: GFAP and NeuN-staining were judged to be the most suitable options for comparative purposes, as they were also employed in a previous histological evaluation of polyimide cylindrical probes in the rat brain [20]. Photomicrographs were obtained by capturing images directly from the sections with a digital camera attached to the microscope and assembled into digital montages by the Nis-element software (Nikon Instruments Inc.). Individual images were then imported in Adobe Photoshop, in which the brightness and contrast of the image were adjusted, if necessary, to reproduce the original histological data.

To evaluate the tissue reaction caused by our probes we quantified the amount of the astroglia reaction and the loss of neurons by using an approach similar to that already employed in previous studies [20, 26, 27]. In particular, GFAP-stained sections were analyzed by focusing on 30 regions of interest (ROIs) for each section (figure 2(B)) and two sections per probe were considered. Each ROI was a square with  $100\ \mu\text{m}$  long sides. Half of the ROIs ( $n = 15$  per sections,  $n = 30$  per probe) were positioned in the third layer and the other half in the fifth layer. Layers were identified using Nissl-stained sections adjacent to the GFAP-stained ones. Because it is known that in some cortical regions the number of cells can differ between these two layers [28], we opted to treat them separately. We introduced the factor Distance (with five levels) grouping all ROIs based on their distance from the edge of the probe track (in each section), from 0 to  $500\ \mu\text{m}$  (in steps of  $100\ \mu\text{m}$ ). The number of the astrocytes in each ROI was counted manually, blind to the location of the ROIs. Then, the number of astrocytes was statistically compared using a repeated measures ANOVA (factor: Distance), with Implant and Layer as additional grouping factors. Bonferroni post-hoc tests ( $p < 0.05$ ) were used where appropriate.



A similar analysis was carried out on the NeuN stained sections. In this latter analysis, since the neurons were more numerous than the astrocytes visualized by GFAP (GFAP delineates only approximately 15% of the total number of the astrocyte; Bushong *et al* [29]), we used a higher number of ROIs of smaller size, 50  $\mu\text{m}$  long sides, relative to those used for GFAP. In particular, NeuN-stained sections were analyzed by focusing on 108 ROIs for each section (figure 2(C)) and two sections per probe were considered. In this case each ROI was a square with a sidelength of 50  $\mu\text{m}$ . Half of the ROIs ( $n = 54$  per sections,  $n = 108$  per probe) were positioned in the third layer and the other half in the fifth layer. Layers were identified

using Nissl-stained sections adjacent to the NeuN-stained ones. As in the case of GFAP analysis, we used the factor Distance (with nine levels) grouping all ROIs based on their distance from the edge of the probe track (in each section), from 0 to 450  $\mu\text{m}$  (in steps of 50  $\mu\text{m}$ ).

The neurons in each ROI were counted, as described above for the GFAP analysis. Then, the number of cells was statistically compared with a repeated measures ANOVA (factor: Distance), using Implant and Layer as additional grouping factors. Bonferroni post-hoc tests ( $p < 0.05$ ) were used in case of significant main or interaction effects involving multiple comparisons.

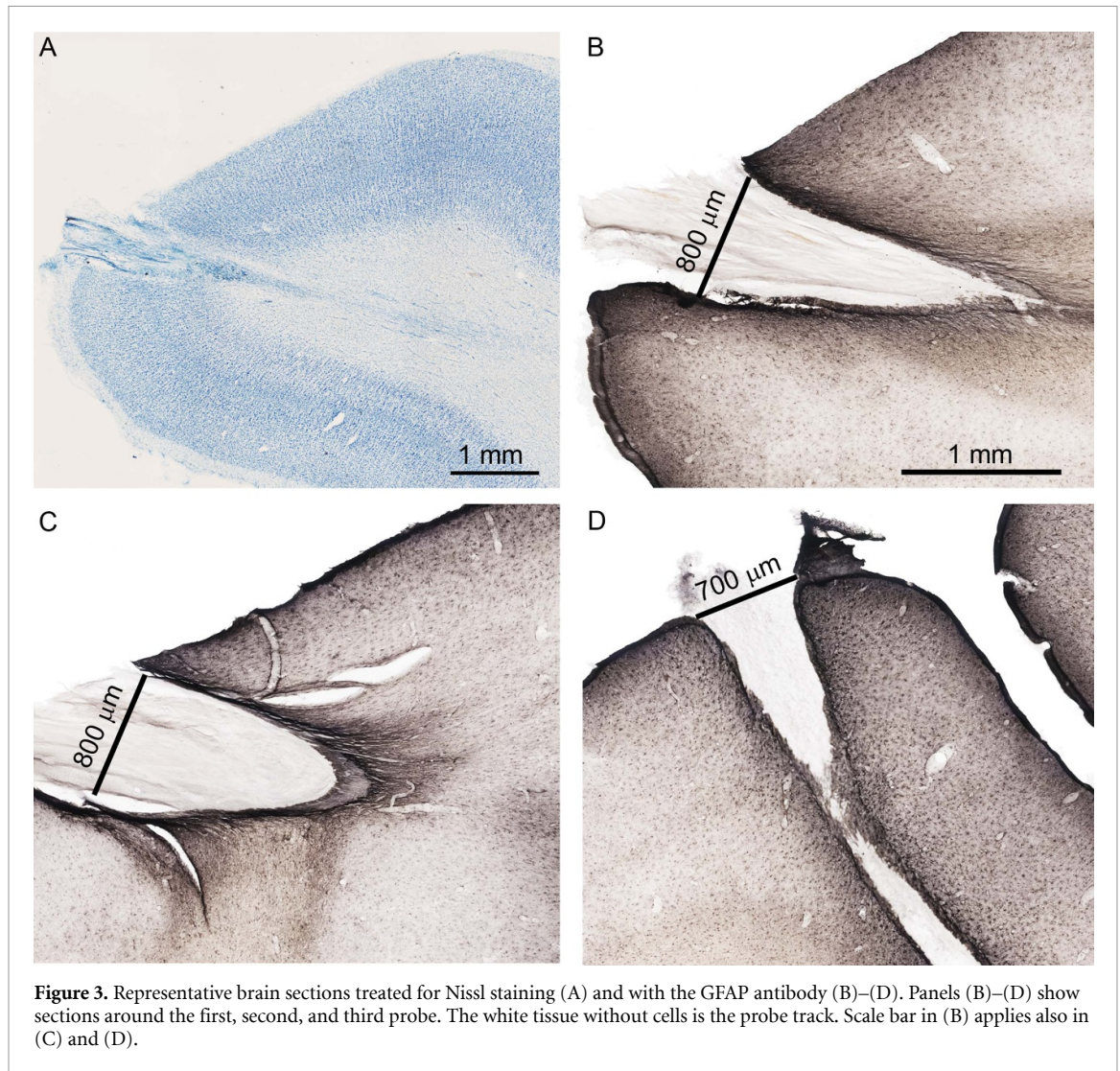


**Figure 3.** Representative brain sections treated for Nissl staining (A) and with the GFAP antibody (B)–(D). Panels (B)–(D) show sections around the first, second, and third probe. The white tissue without cells is the probe track. Scale bar in (B) applies also in (C) and (D).

### 3. Results

#### 3.1. Size of the mechanical lesion

The Nissl stained sections (figure 3(A)) showed that the lesion caused by the Probe was limited to the site of its mechanical insertion. Furthermore, it is clear that the tissue around the probe's track seems to maintain the typical architectonic organization in cortical layers. To quantify in more detail the entity of damage observed in the Nissl stained sections, an analysis of the GFAP- and NeuN-stained sections was carried out.

For all three Probes, GFAP- and Neu-N-stained sections were selected at the level in which the scar tissue (in the case of Probes 1 and 2) or the track in the brain tissue (in the case of Probe 3 removed post-mortem) was larger. In these sections the tissue damage did not exceed 800  $\mu\text{m}$ , corresponding to the probe diameter (figures 3(B)–(D), 4(B), (B1) and (B2)). Sections adjacent (300  $\mu\text{m}$  anterior and 300  $\mu\text{m}$  posterior) to the central ones exhibited negligible tissue damage (figures 4(A), (A1), (A2) and (C1)), except for a small amount of gliosis in the

superficial layers of two sections (figures 4(C) and (C2)).

The count of GFAP immunostained astrocytes in the ROIs located at different distances from the edge of the probe track (in the range 0–500  $\mu\text{m}$ , see Methods) showed a significant main effect only of the factor Distance ( $F = 18.7$ ,  $p < 0.001$ ). Bonferroni post-hoc tests (figure 5(A)) indicated that a greater number of astrocytes was limited to the first ROI (0–100  $\mu\text{m}$ ) close to the probe's track relative to all other distances ( $p < 0.001$  for all comparisons), which in turn did not differ from each other ( $p > 0.096$  for all comparisons). No statistically significant effect was detected for any of the other examined factors that are Layer and Implant (figures 5(C) and (E)). The count of stained neurons in the ROIs located at nine different distances from the probes' track (in the range 0–450  $\mu\text{m}$ , see Methods) showed a significant main effect of the factor Distance ( $F = 49.42$ ,  $p < 0.001$ ). Furthermore, Bonferroni post-hoc tests (figure 5(B)) indicated the presence of lower number of neurons in the first distance relative to all other distances ( $p < 0.001$  for all comparisons), and in the second

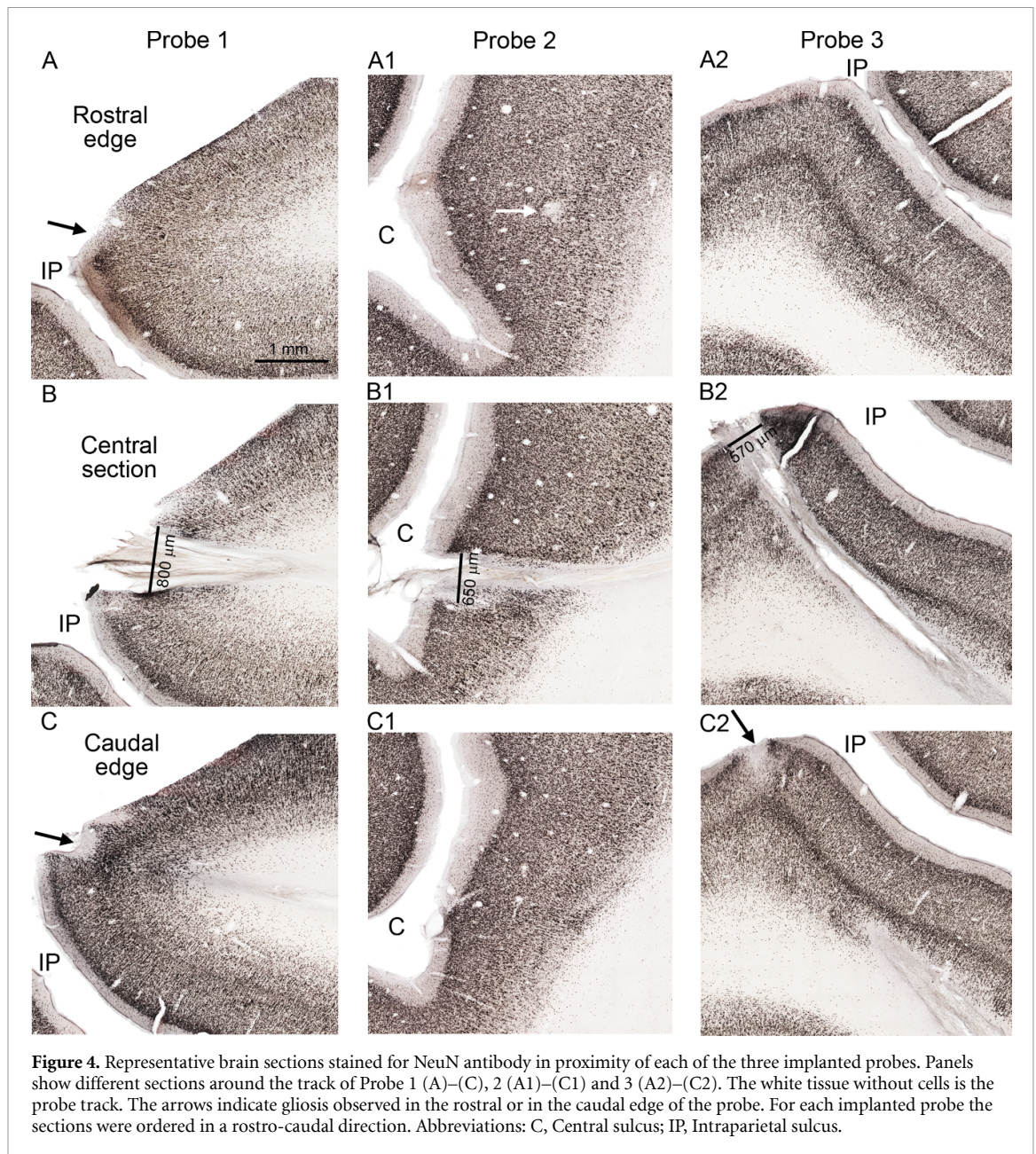


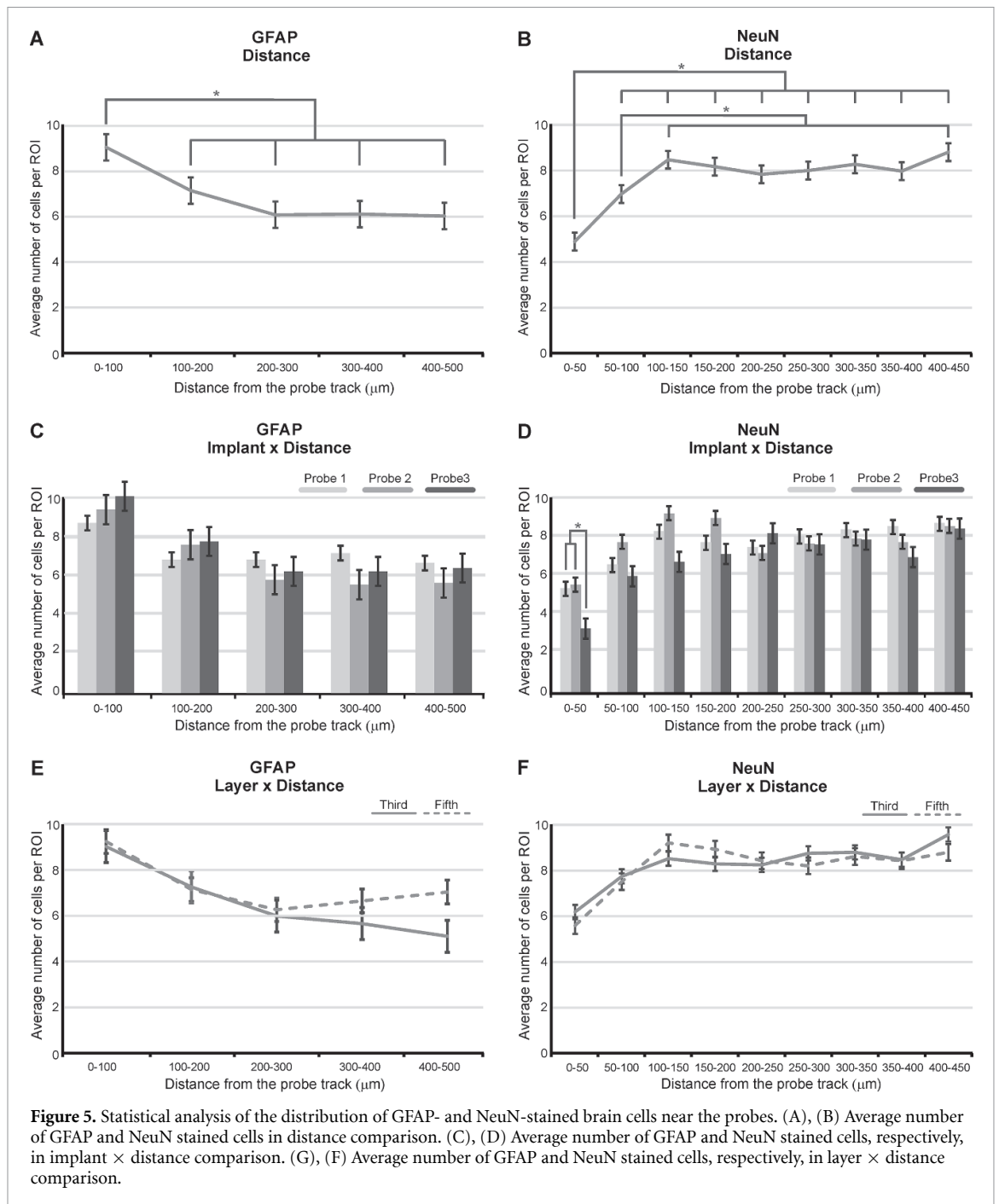
**Figure 4.** Representative brain sections stained for NeuN antibody in proximity of each of the three implanted probes. Panels show different sections around the track of Probe 1 (A)–(C), 2 (A1)–(C1) and 3 (A2)–(C2). The white tissue without cells is the probe track. The arrows indicate gliosis observed in the rostral or in the caudal edge of the probe. For each implanted probe the sections were ordered in a rostro-caudal direction. Abbreviations: C, Central sulcus; IP, Intraparietal sulcus.

relative to the third ( $p = 0.02$ ) and ninth ( $p = 0.001$ ) distance, whereas all the other distances did not differ from each other ( $p > 0.105$  for all comparisons). No statistically significant effect was detected for the factor Layer (figure 5(F)). We also found a significant interaction effect for the factors distance and probe ( $F = 1.903$ ,  $p = 0.020$ ), suggesting a slightly greater reduction in the number of neurons in close proximity (0–50  $\mu\text{m}$ ) of the scar track of Probe 3 relative to all other distances and probes ( $p < 0.01$  for all comparisons; figure 5(D)).

#### 4. Discussion

In this study, we assessed the tissue reaction for recently developed cylindrically shaped neural probes suitable for the recording of LFP, MUA and SUA activity from a few days to several weeks after their

implantation in a non-human primate [6]. The possibility to translate this technology to human use was limited, so far, by the lack of evidence regarding the actual effects of these neural devices on brain tissue. Indeed, data were limited to chronic applications in rats of similar probes, characterized by the same outer diameter but obviously much shorter [20]. Clearly, the length of the probes may affect the probability to intercept blood vessels, it may render them much more unstable in the brain tissue during active movement (like the violent jumping and climbing actions typical of primates) and, potentially, could contribute to greater tissue damage/reaction in a small animal model brain. In contrast with these possible effects, our post-mortem histological analyses allowed us to verify that the mechanical lesion caused by probe implantation is essentially limited to the diameter of the probe, and tissue reaction, in terms of loss of



neurons and proliferation of glial cells, is very limited and confined to the territory in close proximity to the probes' tracks.

Differently from our results, in the aforementioned rat study [20], the authors described in some animals relatively bigger lesions, i.e. 200–300 microns beyond the size of the mechanical damage provoked by the probe, considered as a consequence of hemorrhagic injury caused by disruption of blood vessel occurred during the insertion procedure. The relative size of the probe diameter with respect to the overall size of the animal brain may account for this result. Indeed, the authors found a lower yield of single units in rats with more evident lesions as compared

to non-lesioned animals, coherently with the hypothesis of bleeding damage. In contrast, (a) we did not find relevant sign of hemorrhagic lesion, (b) we could record LFP, MUA, and SUA from a few hours to several weeks following implantation [6] and, (c) we did not observe any relevant neurological sign following probe implantation, in line with the vast and safe application of physically and mechanically similar probes in humans for pre-surgical evaluation of drug resistant epilepsy [30]. The fact that we did not find any evidence of hemorrhagic damage in our histological material does not prove that it cannot occur at all in large brain animals (including humans), because of the small number of implants analyzed here in



a single subject. However, since cylindrical probes have remarkably similar physical and mechanical features (same or smaller diameter and similar length and flexibility) as those used in epileptic surgery [21, 23] and for deep brain stimulation treatment [31], it is reasonable to expect that bleeding side-effects should not be greater than those normally reported in human patients, where they are relatively rare [30–33].

As far as tissue reactions beyond the territory mechanically damaged by probes insertion are concerned, the three probes implanted caused a moderate increase of astrocytes and a modest cell death exclusively within a radius of 100  $\mu\text{m}$  and of 50  $\mu\text{m}$  from the probe track, respectively. Interestingly, these results are similar to those described in rats by Fiath and colleagues [20], as well as to those reported by other authors who tested the effect on the brain tissue of silicon microprobes of smaller size [27, 34, 35]. Altogether, these observations indicate that the bigger size of our polyimide-based probes did not cause any relevant increase in the astrocytes' reaction and/or in neuronal cell death in comparison with smaller probes.

The cylindrical probes contain both macroelectrodes and microelectrodes, so it could be hypothesized that tissue reaction is different depending on the proximity to one or the other type of electrode or to the probe shank. A precise localization of the different electrodes post-mortem, which would enable to address this question, is impossible; however, we found a uniform distribution of the tissue reaction along the probe shank (in the third and fifth layer), making unlikely that the different types of electrodes differentially affect brain tissue.

To our knowledge, there is no exhaustive post-mortem study on tissue reactions in implanted epileptic patients, but some detailed histopathological investigations were conducted in subjects treated with deep brain stimulation [31, 33, 36, 37]. Interestingly, in virtually all these studies, similarly to our results, no relevant hemorrhage or thrombosis along the electrode tracks was found and, importantly, the extent of brain tissue showing astroglia reaction, gliosis and neuronal degeneration usually is in the range or even exceed the one we found in the present work [31, 33, 36, 37].

Summarizing, our results showed that the two probes explanted months before euthanizing the animal left minimal tissue damage beyond the mechanical lesion. Our study fairly exceeds the duration of typical implantation of similar probes in epileptic patients, suggesting that the tested probes are a viable option for patients undergoing the usual period (from 1 to 2 weeks) of pre-surgical clinical monitoring. Regarding Probe 3, the number of neurons near the insertion track was smaller in comparison with those of the other two probes, suggesting that the longer the time from probe

explantation is, the smaller are the histologically-identifiable consequences of mechanical damage. Of course, the unavoidably small number of implants we have been able to analyze did not allow us to draw firm conclusions on this point.

In conclusion, previous observations showed that the PI -based cylindrical depth probes with microelectrodes and macroelectrodes enable high spatial resolution and temporally stable signals over time [6]. In addition, the relatively limited damage of the PI depth probes here observed after implants with a duration that was longer than that of recording sessions performed in human epileptic clinical trials, indicates that these new neural devices are potentially suitable to be tested for SEEG recordings in epileptic human patients.


## Funding

This work was supported by the European Union's framework program FP7/2007-2013 under Grant Agreement 600925 to G A O and P R, and by the European Research Council (ERC) under the European Union's Horizon 2020 research and innovation program with Grant Agreement 678307 (ERC StG) to L B.

## ORCID iDs

M Gerbella  <https://orcid.org/0000-0002-1204-3484>

E Borra  <https://orcid.org/0000-0001-9374-3361>

M Lanzilotto  <https://orcid.org/0000-0002-3854-7875>

A Livi  <https://orcid.org/0000-0002-7968-1026>

L Fogassi  <https://orcid.org/0000-0003-3348-039X>

O Paul  <https://orcid.org/0000-0002-0829-6569>

G A Orban  <https://orcid.org/0000-0002-8179-9584>

P Ruther  <https://orcid.org/0000-0002-7358-003X>

L Bonini  <https://orcid.org/0000-0002-3485-2127>

## References

- [1] Cossu M *et al* 2005 Stereoelectroencephalography in the presurgical evaluation of children with drug-resistant focal epilepsy *J. Neurosurg. Pediatr.* **103** 333–43
- [2] Rodriguez-Oroz M C *et al* 2005 Bilateral deep brain stimulation in Parkinson's disease: a multicentre study with 4 years follow-up *Brain* **128** 2240–9
- [3] Aflalo T *et al* 2015 Decoding motor imagery from the posterior parietal cortex of a tetraplegic human *Science* **348** 906–10
- [4] Avanzini P, Pelliccia V, Lo Russo G, Orban G A and Rizzolatti G 2018 Multiple time courses of somatosensory responses in human cortex *Neuroimage* **169** 212–26
- [5] Ter Wal M *et al* 2020 Human stereoEEG recordings reveal network dynamics of decision-making in a rule-switching task *Nat. Commun.* **11** 1–12
- [6] Pothof F *et al* 2016 Chronic neural probe for simultaneous recording of single-unit, multi-unit, and local field potential activity from multiple brain sites *J. Neural Eng.* **13** 1–13

- [7] Barz F *et al* 2017 Versatile, modular 3D microelectrode arrays for neuronal ensemble recordings: from design to fabrication, assembly, and functional validation in non-human primates *J. Neural Eng.* **14** 036010
- [8] Luan L *et al* 2017 Ultraflexible nanoelectronic probes form reliable, glial scar-free neural integration *Sci. Adv.* **3** e1601966
- [9] Raducanu B C *et al* 2017 Time multiplexed active neural probe with 1356 parallel recording sites *Sensors* **17** 2388
- [10] Ferroni C G, Maranesi M, Livi A, Lanzilotto M and Bonini L 2017 Comparative performance of linear multielectrode probes and single-tip electrodes for intracortical microstimulation and single-neuron recording in macaque monkey *Front. Syst. Neurosci.* **15** 11:84
- [11] Wu F, Stark E, Ku P-C, Wise K D, Buzsáki G and Yoon E 2015 Monolithically integrated  $\mu$ LEDs on silicon neural probes for high-resolution optogenetic studies in behaving animals *Neuron* **88** 1136–48
- [12] Ayub S *et al* 2020 Compact optical neural probes with up to 20 integrated thin-film LEDs applied in acute optogenetic studies *IEEE Trans. Biomed. Eng.* **67** 2603–15
- [13] Misra A *et al* 2014 Methods for implantation of micro-wire bundles and optimization of single/multi-unit recordings from human mesial temporal lobe *J. Neural Eng.* **11** 026013
- [14] Worrell G A *et al* 2008 High-frequency oscillations in human temporal lobe: simultaneous microwire and clinical macroelectrode recordings *Brain* **131** 928–37
- [15] Kutter E F, Bostroem J, Elger C E, Mormann F and Nieder A 2018 Single neurons in the human brain encode numbers *Neuron* **100** 753–61
- [16] Carlson A A, Rutishauser U and Mamelak A N 2018 Safety and utility of hybrid depth electrodes for seizure localization and single-unit neuronal recording *Stereotact. Funct. Neurosurg.* **96** 311–19
- [17] Lotti F, Ranieri F, Vadalà G, Zollo L and Di Pino G 2017 Invasive intraneural interfaces: foreign body reaction issues *Front. Neurosci.* **6** 11:497
- [18] Petrini F M *et al* 2019 Six-month assessment of a hand prosthesis with intraneural tactile feedback *Ann. Neurol.* **85** 137–54
- [19] Rubehn B, Bosman C, Oostenveld R, Fries P and Stieglitz T 2009 A MEMS-based flexible multichannel ECoG-electrode array *J. Neural Eng.* **6** 036003
- [20] Fiáth R *et al* 2018 Long-term recording performance and biocompatibility of chronically implanted cylindrically-shaped, polymer-based neural interfaces *Biomed. Tech.* **63** 301–15
- [21] Isnard J, Guénot M, Sindou M and Mauguière F 2004 Clinical manifestations of insular lobe seizures: a stereo-electroencephalographic study *Epilepsia* **45** 1079–90
- [22] Cardinale F, Casaceli G, Raneri F, Miller J and Lo Russo G 2016 Implantation of stereoelectroencephalography electrodes: a systematic review *J. Clin. Neurophysiol.* **33** 490–502
- [23] Caruana F *et al* 2018 Motor and emotional behaviours elicited by electrical stimulation of the human cingulate cortex *Brain* **141** 3035–51
- [24] Lanzilotto M *et al* 2019 Anterior intraparietal area: a hub in the observed manipulative action network *Cereb. Cortex* **29** 1816–33
- [25] Lanzilotto M, Maranesi M, Livi A, Ferroni C G, Orban G A and Bonini L 2020 Stable readout of observed actions from format-dependent activity of monkey's anterior intraparietal neurons *Proc. Natl Acad. Sci. USA* **117** 16596–605
- [26] Azemi E, Lagenaur C F and Cui X T 2011 The surface immobilization of the neural adhesion molecule L1 on neural probes and its effect on neuronal density and gliosis at the probe/tissue interface *Biomaterials* **32** 681–92
- [27] Bérces Z *et al* 2016 Neurobiochemical changes in the vicinity of a nanostructured neural implant *Sci. Rep.* **6** 1–11
- [28] Gerbella M, Belmalih A, Borra E, Rozzi S and Luppino G 2007 Multimodal architectonic subdivision of the caudal ventrolateral prefrontal cortex of the macaque monkey *Brain Structure & Function* (available at: [www.ncbi.nlm.nih.gov/pubmed/17899184](http://www.ncbi.nlm.nih.gov/pubmed/17899184)) (Accessed 16 November 2012)
- [29] Bushong E A, Martone M E, Jones Y Z and Ellisman M H 2002 Protoplasmic astrocytes in CA1 stratum radiatum occupy separate anatomical domains *J. Neurosci.* **22** 183–92
- [30] Tandon N *et al* 2019 Analysis of morbidity and outcomes associated with use of subdural grids vs stereoelectroencephalography in patients with intractable epilepsy *JAMA Neurol.* **76** 672–81
- [31] Boivie J and Meyerson B A 1982 A correlative anatomical and clinical study of pain suppression by deep brain stimulation *Pain* **13** 113–26
- [32] Fong J S, Alexopoulos A V, Bingham W E, Gonzalez-Martinez J and Prayson R A 2012 Pathologic findings associated with invasive EEG monitoring for medically intractable epilepsy *Am. J. Clin. Pathol.* **138** 506–10
- [33] Van Kuyck K, Welkenhuysen M, Arckens L, Sciôt R and Nuttin B 2007 Histological alterations induced by electrode implantation and electrical stimulation in the human brain: a review *Neuromodulation* **10** 244–61
- [34] Biran R, Martin D C and Tresco P A 2005 Neuronal cell loss accompanies the brain tissue response to chronically implanted silicon microelectrode arrays *Exp. Neurol.* **195** 115–26
- [35] Winslow B D and Tresco P A 2010 Quantitative analysis of the tissue response to chronically implanted microwire electrodes in rat cortex *Biomaterials* **31** 1558–67
- [36] Haberler C *et al* 2000 No tissue damage by chronic deep brain stimulation in Parkinson's disease *Ann. Neurol.* **48** 372–6
- [37] Henderson J M *et al* 2002 Postmortem analysis of bilateral subthalamic electrode implants in Parkinson's disease *Mov. Disord.* **17** 133–7